The Impacts of Co and Ni Additions to High Solute Content Fe-Contaminated Al alloys in Beneficing Microstructure and Tensile Properties

Marcella Gautê Cavalcante Xavier[a], José Eduardo Spinelli[b] *

[a] Universidade Federal de São Carlos (UFSCar), Programa de Pós-Graduação em Ciência e Engenharia de Materiais, São Carlos, SP, Brasil.
[b] Universidade Federal de São Carlos (UFSCar), Departamento de Engenharia de Materiais, 13565-905, São Carlos, SP, Brasil.

The accumulation of tramp impurities, particularly Fe, during recycling of Al alloys frequently leads to the production of coarse intermetallics during solidification, which affect final product mechanical properties. Because lowering the Fe concentration and/or using thermomechanical processing to subdivide the particles is expensive, it is preferred to modify the morphology, size, and distribution of the IMCs during solidification. Benefiting the properties of Al-contaminated alloys entails increased recyclability and a reduction in the usage of virgin primary Al and downcycled alloys. The Al-8%Si-0.8%Fe-2.5%Cu-1.0%Zn (in wt.%) alloy was modified with 0.7%Ni and 0.7%Co. Both dendritic growth and tensile properties were evaluated for the three alloys. The secondary dendrite arm spacing values (λ_2) were found very refined for all alloys. The λ_2 in the modified alloys was even more reduced. The Co addition of 0.7% reached higher values of tensile strength (220 MPa) as compared to the others without major losses in ductility. The addition of Co can enhance strength by up to 15%, considering more refined microstructures.

Keywords: *Recycling aluminum alloys, solidification, AlFeSi intermetallics, tensile properties*

1. Introduction

To meet aerospace, automotive, and construction material needs, a cost-effective abundant material with specific properties is essential. Currently, Al alloys fulfill these requirements and find extensive application. To lower carbon impact, recycling or incorporating recycled Al in production is considered. However, recycling can lead to detrimental intermetallic compound (IMC) formation due to impurities like Fe.

Al demand is rising as raw materials deplete; recycling gains importance. Industrial Al alloy use is growing, projected to double by 2050, primarily in transport, electric, construction, and packaging sectors[1]. The Al industry must cut emissions by 80% by 2050[2,3]. Al alloys' carbon footprint mainly stems from primary production (5-19 tCO_2 eq / t), while post-consumer scrap is much lower (~0.5 tCO_2 eq / t). Incorporating recycled content in alloy production is vital for greener, sustainable Al.

To counter Fe contamination in Al scrap, strategies typically involve downcycling or increased primary Al use. Much research has focused on enhancing Fe tolerance in Al-Fe alloys by manipulating phase morphologies, distributions, and sizes[4,5]. Research on coarse primary intermetallics in high-Fe content alloys is crucial, involving Ni and Co alloying, solidification kinetics, intermetallic characterization (morphology, growth, anisotropy, hardness), and impact on mechanical properties and corrosion. Proposing new solidification pre-programming operations and setups may

be more sustainable in the sense that scraps become more recyclable, reducing the use of virgin Al and increasing upcycling opportunities.

Recyclability assessment hinges on scrap types and chemical compositions, crucially impacting Al alloy production[6]. Certain alloys like 380 alloy for die casting can incorporate more contaminated scraps (up to 3-4% Cu, 2% Fe, 3% Zn). Creating "recycling-friendly" alloys is a 21st-century engineering challenge since secondary Al production consumes significantly less energy than primary Al. Given that 75% of Al products is still in use, Al recycling acquires importance and sustainability as scrap variety and volume increase[7-9]. Controlling the Fe content of Al scrap-derived alloys is critical, yet limiting Fe while employing a high quantity of virgin Al contradicts environmental goals. Fe addition in Al alloys serves various purposes, including enhancing mechanical properties at high temperatures and mold durability in casting with steel molds[10]. It is yet unclear how to improve alloy properties and make more Fe-tolerant, recyclable alloys in a more sustainable way by modifying the solidification procedures used in Al-Si based alloys to involve elements such as Ni, Co, and Mn.

Commercially pure Al consists of around 99.2 wt.% Al with impurities; e.g., 0.3% Fe and 0.2% Si. These levels surpass solubility limits, promoting AlFeSi intermetallic formation during solidification. Si contributes to hexagonal α-Al_8Fe_2Si and monoclinic/orthorhombic β-Al_5FeSi phases, potentially increasing with higher Fe content. Mn and Si with Fe generate $Al_{15}(Fe, Mn)_3Si$ cubic phase. Uncommon phases can emerge with Ni, Co, Cu, and Be[11-13].

*e-mail: spinelli@ufscar.br

Some studies introduced alloying elements for intermetallic control. Sha et al.[14] added Co to neutralize β phase in Al-20%Si-2%Cu-1%Ni-0.7Co alloys, morphing into Chinese script $Al_{15}(Fe, Co, Ni)_3Si$. 0.3% and 0.5% Ni in AlSi10MgMn alloy containing 1% Fe improved microstructure, tensile strength, and ductility[15]. Ni destabilized Fe-containing β-phase in recycled Al-Si cast alloys[16]. It remains unclear how Co and Ni additions can be efficient on modifying Fe-containing phases in high-Fe content alloys. Dendritic and eutectic growth, AlFe intermetallic composition, growth mode, and anisotropy under diverse solidification conditions warrant investigation for varied Al-Si based scraps[17].

The novelty of the present study lies in assessing the efficiency of the additions of Ni and Co in high-alloyed Al scrap contaminated with Fe. More importantly, it involves examining these impacts on microstructure and tensile properties across a broad range of solidification conditions, representing an analogy to parameters related to various industrial processing methods. There are no records in the literature of detailed scrap correction studies like this.

Engineering studies may optimize alloy performance, assisting recycling to prevent downcycling and virgin Al use. Altering intermetallic morphology and distribution in solidification offers a cost-effective recycling fix. The present work aims to investigate the impacts of Ni and Co on microstructure and tensile properties in Al-8%Si-0.8%Fe-2.5%Cu-1.0%Zn (scrap) alloy samples solidified at different solidification cooling rates. Experimental correlations between secondary dendritic spacing and cooling rate; and between strength and secondary dendritic spacing will be given. It is a first step towards elevating recyclability and curbing Fe-contaminated scrap's environmental impact. The results address significant issues with solidification process improvement.

2. Experimental Procedure

Al-Si alloys with high alloy contents were processed using an unsteady-state setup. The Al-8%Si-0.8%Fe-2.5%Cu-1.0%Zn, Al-8%Si-0.8%Fe-2.5%Cu-1.0%Zn-0.7%Ni and Al-8%Si-0.8%Fe-2.5%Cu-1.0%Zn-0.7%Co (in wt.%) alloys were manufactured from commercial pure elements (>99.79 mass%), and characterized and tested in the "as-cast" conditions. This directional solidification device, as described in previous research works[18,19], is water-cooled on the bottom surface of the carbon steel plate 1020 situated at its base. This allowed varied cooling rates to be achieved over the entire length of the ingot.

Portions of these alloys, previously melted by induction furnace, were poured into a cylindrical stainless steel mold attached to the directional solidification device (DS). Upon reaching the desired conditions of the liquid metal, i.e., overheating temperatures above 5% of the liquidus temperature of each alloy, the cooling system was activated, allowing the initiation of upward vertical solidification. The evolution of temperatures along the length of the casting was monitored by fine K-type thermocouples positioned in distinct quotas until 70 mm from the bottom surface. The temperature device allowed very accurate data acquisition of 5 Hz on each thermocouple for both cooling curve and directional solidification thermal profiles.

The microstructures formed under different solidification conditions were assessed. This process includes the evaluation of both longitudinal and transverse samples from each measurement position. The characterization technique using optical microscopy (OM) allowed for the observation of the microstructure and its quantification based on the length measurements of the formed structure (in all cases, dendritic matrix). Measurements on the as-solidified microstructure were conducted using the line-intercept method[20] for secondary dendrite arm spacings, λ_2. At least 40 measurements were performed for each selected position along each casting.

Advanced characterization of the microstructures, morphologies and compositions of the phases was carried out through SEM analyses. In order to enable the observation of the morphological details, deep-etched samples were prepared (HCl during 1 min). The equipment used was a Philips SEM (XL-30 FEG), which is coupled with an energy-dispersive X-ray spectrometer (EDS).

For the determination of tensile mechanical properties, transverse samples were extracted from different positions along the solidified ingots. To ensure the reproducibility of results in the tensile tests, four specimens were taken for each position to determine the ultimate tensile strength (σ_u) and elongation at fracture (δ). The specimens were prepared in accordance with ASTM Standard E 8M/16a[21] specifications and tested on an Instron 5500R machine at a nominal strain rate of 3×10^{-3} s^{-1}.

3. Results and Discussions

The experimental temperature data varying over time were recorded for the 3 alloys. In this way, it was possible to determine the solidification rates according to Figure 1 for the different thermocouples inserted in the alloys. A single correlation for the Al–8%Si–0.8%Fe–2.5%Cu–1.0%Zn-0.7%Co and Al–8%Si–0.8%Fe–2.5%Cu–1.0%Zn-0.7%Ni alloys described the experimental trends along the positions. Higher cooling rates are observed for the alloys modified with Co (21 °C/s) and Ni (14 °C/s).
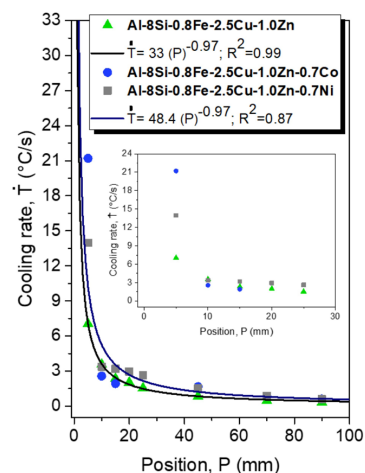
Figure 1. Cooling rate variations in the Al-8%Si-0.8%Fe-2.5%Cu-1.0%Zn, Al-8%Si-0.8%Fe-2.5%Cu-1.0%Zn-Ni and Al-8%Si-0.8%Fe-2.5%Cu-1.0%Zn-Co alloy castings.

Cooling rate during solidification is an essential parameter as it directly influences the microstructure and properties of the alloy. A higher cooling rate typically results in finer spacing and improved mechanical properties. It affects the formation of crystal structures, phase transformations, and the distribution of alloying elements, influencing the final product's strength, hardness, and other properties as corrosion and wear. Control over the cooling rate is essential in various manufacturing processes, including casting and welding, to achieve desired properties and performance. We measured cooling rate and it is clear that Co and Ni increased cooling rate in the very first solid layers (< 10 mm) formed from the bottom of the casting. More experiments under faster cooling would be necessary for a more precise explanation as well as other parameters related to these alloys should be determined. Cooling rate depends on metal/mold wettability, solidification interval and thermal diffusivity[22,23]. Co and Ni are probably changing one or more of these factors. A detail of the plots up to 30 mm was included as an inset and shows that the unmodified alloy has lower cooling rates in this range of the casting.

Microstructures in different ingot positions arise from varying cooling rate along their length. Figure 2 shows evolving dendritic α-Al morphology in Al-8%Si-0.8%Fe-2.5%Cu-1.0%Zn, Al-8%Si-0.8%Fe-2.5%Cu-1.0%Zn-0.7%Co, and Al-8%Si-0.8%Fe-2.5%Cu-1.0%Zn-0.7%Ni alloys.

Bright regions indicate Al-rich phases, while darker parts contain Fe and Si. High cooling rate samples values foster dense branching, lowering λ_2.

Alloys with high solute content (as it is the case here) exhibit less distinct dendrites. Seen in Al-Si-Zn alloys, a study[24] found seaweed-like dendritic growth, secondary branches forming $<90°$ angles with the primary branch for Al-7%Si-(10, 15, 20)Zn alloys. Zn may affect interdendritic areas in Al-9%Si alloys, lessening distinctness. Zn impact on primary α-Al was reported to be related either to Zn amount or to cooling severity level[24]. Overall, dendritic arrangements in Al alloys with high solute content may exhibit higher refinement than those formed in dilute alloys. Solute buildup at the solidification interface enhances α-Al instability, increasing microstructural refinement.

As can be seen in Figure 3 a behavior distinction between alloys with and without Co and Ni additions appears to apply to the λ_2 correlations with thermal solidification parameters. λ_2 in Co and Ni modified alloys could be expressed through unique correlations, indicating these elements refined dendritic branching. Rejection of denser Ni and Co in the interdendritic liquid most likely induce a flow in the interdendritic channel towards the dendrite base. This flow destabilizes primary dendrite side walls, leading to increased secondary branching and reduced λ_2[25].
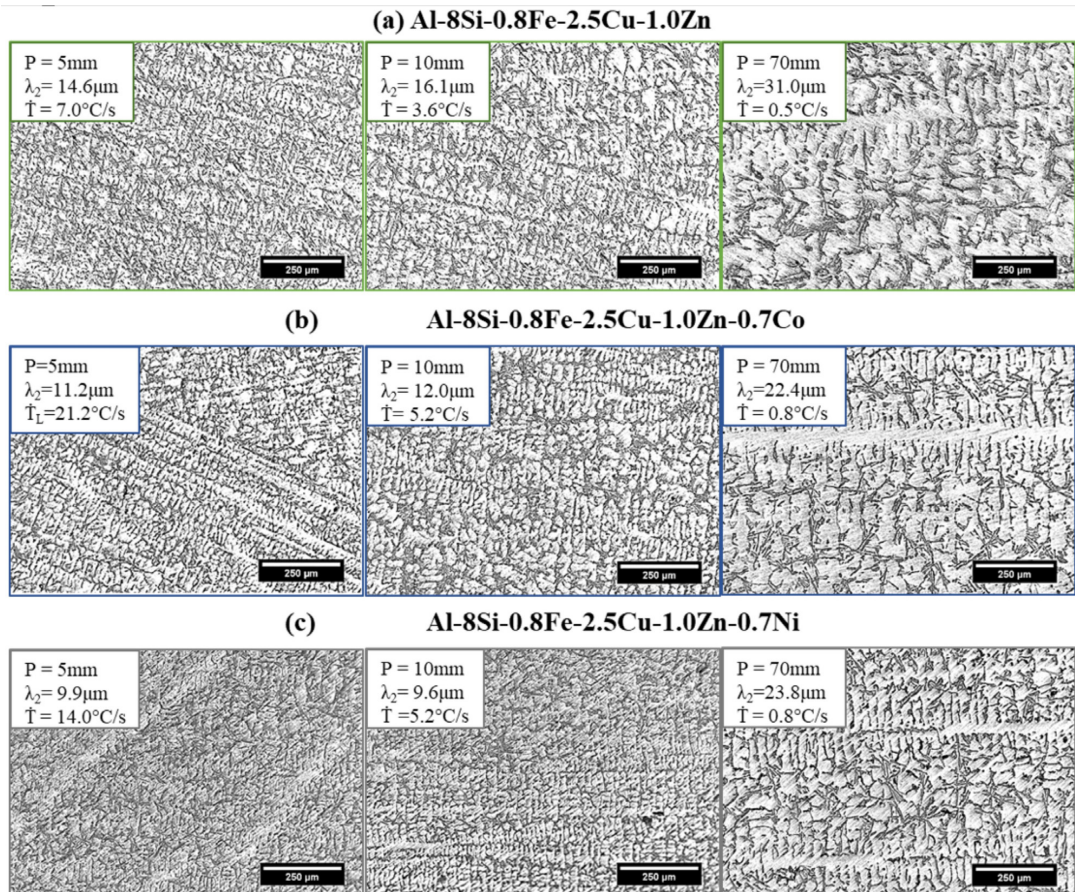
Figure 2. Microstructures of the longitudinal sections observed in the (a) Al-8%Si-0.8%Fe-2.5%Cu-1.0%Zn, (b) Al-8%Si-0.8%Fe-2.5%Cu-1.0%Zn-Co and (c) Al-8%Si-0.8%Fe-2.5%Cu-1.0%Zn-Ni alloy castings.

Regarding to the microstructural details, SEM/EDS analyses and results of the various phases formed can be seen in Figure 4. According to Gowri and Samuel[26] the presence of a high number of alloying elements in Al-Si based alloys complicates the solidification paths with a high number of phases possibly being formed. Si plates are commonly distributed in interdendritic regions very close to the AlFeSi phases, as can be seen in Figure 4. These two phases collectively constitute the majority of the formed interdendritic phases. Rounded phases characterize the Al_2Cu intermetallics in the non-modified alloy. The presence of Co and Ni is observed in some other formed phases beside AlFeSi, such as AlCuFe and the AlCuNi.

Comparing the AlFeSi phases in the alloys containing Co and Ni for a same λ_2 (Figure 4d *vs.* Figure 4f), needles are thinner and longer for Ni, which could have affected the tensile properties. The sharp tips of these needles are acting as stress concentrators, progressively reducing the ultimate tensile strength of the Ni-containing alloy.

Figure 5 presents Thermo-Calc property diagrams illustrating the mass fraction of each stable phase in the alloys, respectively, plotted as a function of temperature in the range of 200-650 °C. As observed, the solidification of the non-modified and of the Ni-containing alloys begins with the formation of the primary α-Al phase (FCC_A1) while the Co-containing alloy computations express initially the formation of the Al_9Co_2 phase. This phase was not found during SEM microscopy analysis in Figure 4. It seems there could be a competition between the α-Al and AlCo primary phases. Given the low fraction of the Al_9Co_2 phase at comparable nucleation temperatures, the experimental results indicate a predominance of the α-Al phase. With the exception of the binary AlNi and AlCo intermetallics, the other phases found in the SEM-EDS analysis were confirmed.

In all cases the fraction of α-Al phase increases almost linearly (while the fraction of liquid decreases linearly) until the temperature reaches a level for other phases to nucleate. At this point, Si (DIAMOND_A4) and AlFeSi (AL9FE2SI2) phases start to grow under equilibrium. Subsequently, transformation in the solid state occurs for AlCu (AL2CU_C16) and AlCu based (AL7CU4NI) phases. While the predicted fractions of Si and AlFeSi phases maintained mostly unaffected for all alloys, with a fraction of 7.7% and 3.0%, at approximately 225°C, respectively, α-Al fractions were predicted to change slightly.

Figure 6 reveals that adding Co to alloy of interest seems to notably enhance tensile strength, reaching 220 MPa, whereas the Ni alloy reached around 195 MPa. Experimental variations in ultimate tensile strength (σ_u) and elongation (δ) were also correlated via Hall-Petch-like functions (σ_u, δ vs. $\lambda_2^{-1/2}$). Tensile strengths of the three alloys improved with a decrease in λ_2 from 32.5 μm to 6 μm. However, the Co and Ni additions seemingly had no impact on δ values, as these values remained unchanged, staying close to 10% throughout all solidified ingots.

According to Gerbe et al.[27], microstructural barriers, such as interdendritic eutectic regions or intermetallic phases, impede the progression of cracks. The significance of the size, nature, and spacing of these microstructure features lies in their impact on mechanical strength, particularly in terms of enhancing failure tolerance. The crack-blocking influence of interdendritic areas bears a resemblance to the effect observed in grain boundaries in polycrystalline alloys. In this context, the λ_2 can be viewed as an analogy to grain size, drawing parallels to the Hall-Petch relationship. This explains why λ_2 reduction gives higher strength values. Furthermore, the alloy containing Co was examined for the presence of smaller AlFeSi particles that could potentially augment their strength in comparison to other alloy compositions. Ductility was not affected by Co or Ni or λ_2. This property appears to be more closely linked to the fractions of the more ductile α-Al phase, which remained quite similar for all three alloys, around 83-85%, according to the calculations via Thermo-Calc in Figure 5. In other words, tensile strength is controlled by the nature and size of the interdendritic phases, while ductility is influenced by the α-phase fraction.
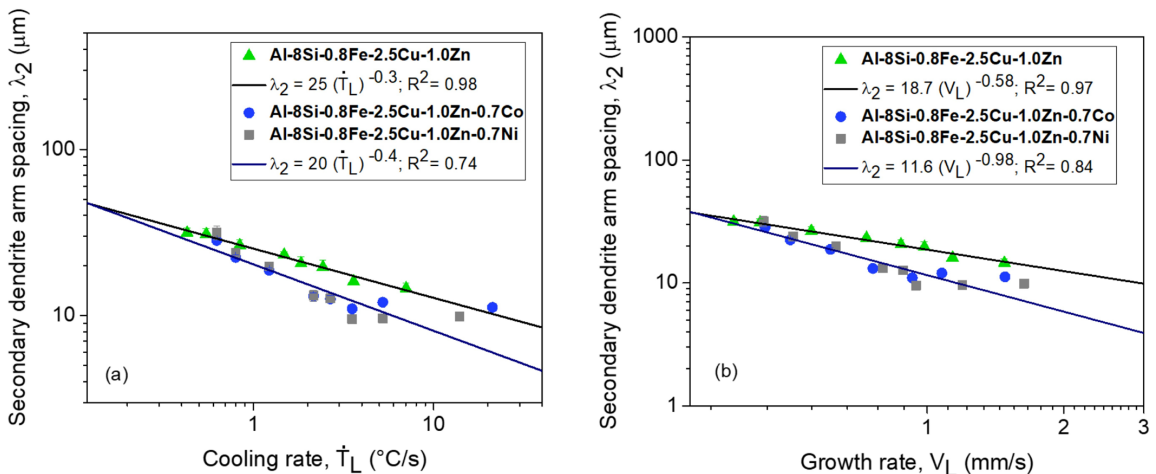

Figure 3. Experimental relationships for λ_2 in Al-8%Si-0.8%Fe-2.5%Cu-1.0%Zn-0.7%(Co, Ni) alloys: (a) λ_2 vs. cooling rate and (b) λ_2 vs. growth rate.

Our findings highlight the benefits of adding cobalt to the studied alloy composition. Globally, cobalt production has reached 197,791 tonnes in 2022, with the electric vehicle (EV) industry being the largest consumer, accounting for around 40% of total demand. The rapid growth of the EV sector is expected to double global cobalt demand by 2030[28]. Despite the increasing consumption of cobalt, there are also promising opportunities for enhancing end-of-use recycling.

Companies are optimistic about the potential for improving the recycling of cobalt in various end-use product forms[29]. The main challenge remains in expanding the secondary cobalt supply from superalloys, vehicles, consumer electronics, cemented carbides, and magnets. Besides recycling operations, for this demand to be met, future Co supply must become more diversified geographically and mined more as a byproduct of Ni over next years[28].
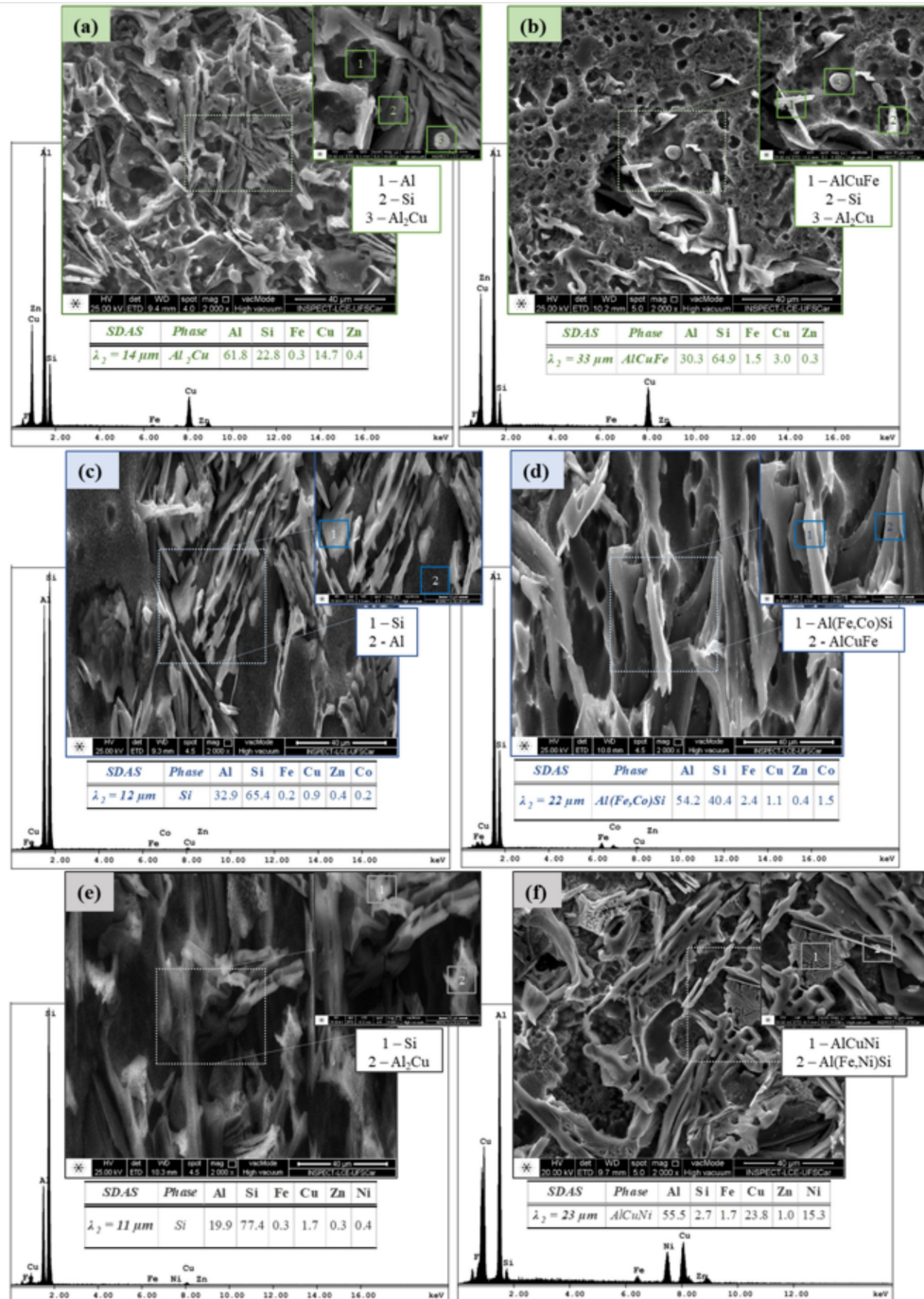
Figure 4. SEM microstructures of (a,b) non-modified, (c,d) Co and (e,f) Ni containing Al-Si-Fe-Cu-Zn alloys. The chemical compositions of the phases are given in atomic percent (at. %). SDAS means secondary dendrite arm spacing.
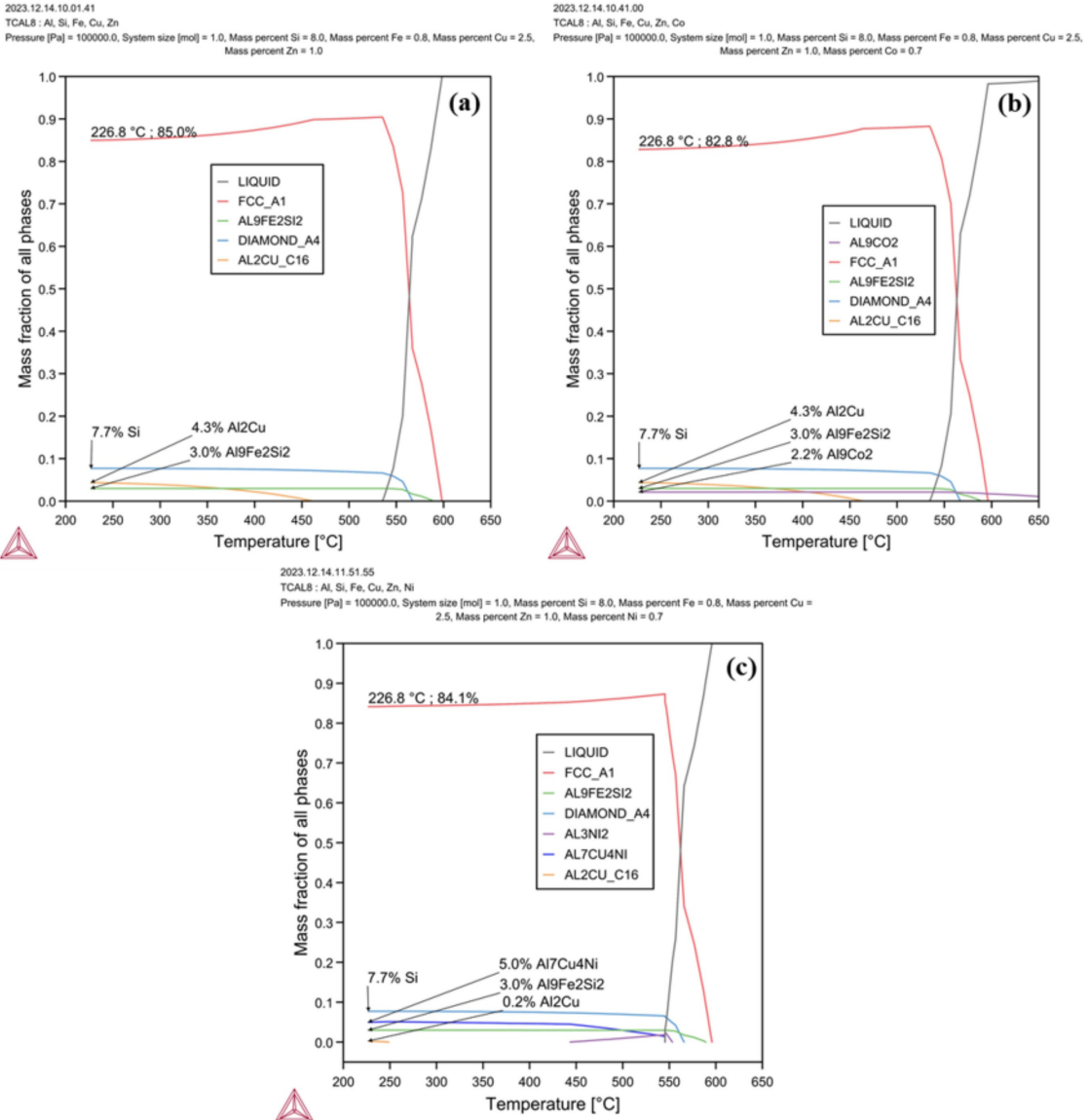
Figure 5. Solidification paths of the alloys using the equilibrium plots provided by Thermo-Calc TCAL8: (a) Al-8%Si-0.8%Fe-2.5%Cu-1.0%Zn, (b) Al-8%Si-0.8%Fe-2.5%Cu-1.0%Zn-0.7%Co, and (c) Al-8%Si-0.8%Fe-2.5%Cu-1.0%Zn-0.7%Ni.
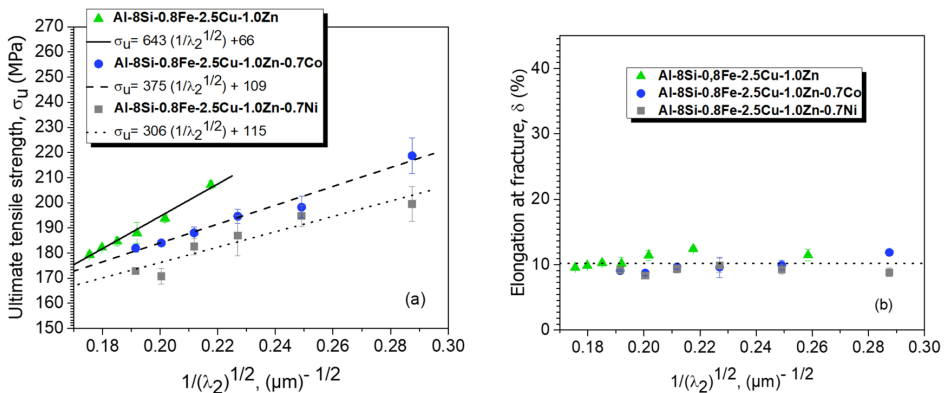
Figure 6. Experimental Hall-Petch-type relationships: (a) tensile strength and (b) elongation at fracture as a function of λ_2.

4. Conclusions

In this study, temperature data were collected for three different alloys, allowing for the determination of the solidification cooling rates. The data revealed that alloys modified with Co and Ni exhibited higher cooling rates as compared to the non-modified alloy. Microstructural analysis demonstrated that the presence of Co and Ni led to refined dendritic branching, affecting the λ_2 experimental correlations. SEM/EDS analysis identified various phases in the alloys, with the presence of Co and Ni influencing the characteristics of the AlFeSi phase. Tensile strength testing showed that Co addition enhanced tensile strength compared to Ni, with a Hall-Petch-like relationship derived between λ_2 and tensile strength.

5. Acknowledgements

6. References

1. International Aluminium Institute. Opportunities for aluminium in a post-Covid economy. London; 2022.
2. Bertram, M. Monday stats post. London: International Aluminium Institute; 2001. 29 p.
3. Cru International Limited. Opportunities for aluminium in a post-Covid economy. London: International Aluminium Institute; 2022. 41 p.
4. Puncreobutr C, Phillion AB, Fife JL, Rockett P, Horsfield AP, Lee PD. In situ quantification of the nucleation and growth of Fe-rich intermetallics during Al alloy solidification. Acta Mater. 2014;79:292-303. http://dx.doi.org/10.1016/j.actamat.2014.07.018.
5. Basak CB, Babu NH. Influence of Cu on modifying the beta phase and enhancing the mechanical properties of recycled Al-Si-Fe cast alloys. Sci Rep. 2017;7(1):1-10. http://dx.doi.org/10.1038/s41598-017-05937-2. PMid:28127051.
6. Gaustad G, Olivetti E, Kirchain R. Design for recycling. J Ind Ecol. 2010;14(2):286-308. http://dx.doi.org/10.1111/j.1530-9290.2010.00229.x.
7. Jiang W, Chen X, Wang B, Fan Z, Wu H. Effects of vibration frequency on microstructure, mechanical properties, and fracture behavior of A356 aluminum alloy obtained by expendable pattern shell casting. Int J Adv Manuf Technol. 2016;83(1-4):167-75. http://dx.doi.org/10.1007/s00170-015-7586-0.
8. Bulkley JW, Keoleian GA, Kar K, Manion M. Industrial ecology of the automobile: a life cycle perspective. Warrendale: SAE; 1997.
9. Maung KN, Yoshida T, Liu G, Lwin CM, Muller DB, Hashimoto S. Assessment of secondary aluminum reserves of nations. Resour Conserv Recycling. 2017;126:34-41. http://dx.doi.org/10.1016/j.resconrec.2017.06.016.
10. Mondolfo LF. Aluminum alloys: structure and properties. Oxford: Butterworths; 1976.
11. Campbell J. Castings. Oxford: Butterworth-Heinemann; 1991.
12. Zolotorevsk VS, Belov NA, Glazoff MV. Casting aluminum alloys. 1st ed. USA: Elsevier Ltd.; 2007. Chapter 5, Industrial casting aluminum alloys; p. 327-96. http://dx.doi.org/10.1016/B978-008045370-5.50007-9.
13. Rana RS, Purohit R, Das S. Reviews on the influences of alloying elements on the microstructure and mechanical properties of aluminum alloys and aluminum alloy composite. Int J Scient Res Pub. 2012;2:1-7.
14. Sha M, Wu S, Wan L. Combined effects of cobalt addition and ultrasonic vibration on microstructure and mechanical properties of hypereutectic Al–Si alloys with 0.7% Fe. Mater Sci Eng A. 2012;554:142-8. http://dx.doi.org/10.1016/j.msea.2012.06.026.
15. Žihalova M, Bolibruchová D, Matejka M. Change in the microstructure of AlSi10MgMn alloy with higher iron content due to an increase in the amount of nickel. Teh Vjesn. 2021;2(1)8:34-7.
16. Basak CB, Meduri A, Hari Babu N. Influence of Ni in high Fe containing recyclable Al-Si cast alloys. Mater Des. 2019;182:108017. http://dx.doi.org/10.1016/j.matdes.2019.108017.
17. Feng S, Cui Y, Liotti E, Lui A, Gourlay CM, Grant PS. In-situ X-ray radiography of twinned crystal growth of primary Al13Fe4. Scr Mater. 2020;184:57-62. http://dx.doi.org/10.1016/j.scriptamat.2020.04.010.
18. Cruz CB, Kakitani R, Xavierb MGC, Silva BL, Garcia A, Cheung N, et al. Transient unidirectional solidification, microstructure and intermetallics in Sn-Ni alloys. Mater Res. 2018;21(Suppl 1):1-11. http://dx.doi.org/10.1590/1980-5373-mr-2017-1099.
19. Reyes RAV, Garcia A, Spinelli JE. Evaluating microstructure, wear resistance and tensile properties of Al-Bi(-Cu, -Zn) alloys for lightweight sliding bearings. Metals. 2021;11(1):153. http://dx.doi.org/10.3390/met11010153.
20. McCartney DG, Hunt JD. Measurements of cell and primary dendrite arm spacings in directionally solidified aluminium alloys. Acta Metall. 1981;29(11):1851-63. http://dx.doi.org/10.1016/0001-6160(81)90111-5.
21. ASTM: American Society for Testing and Materials. ASTM E8/E8M-16a: standard test methods for tension testing of metallic materials. West Conshohocken: ASTM; 2016.
22. Cheung N, Santos NS, Quaresma JMV, Dulikravich GS, Garcia A. Interfacial heat transfer coefficients and solidification of an aluminum alloy in a rotary continuous caster. Int J Heat Mass Transf. 2009;52(1-2):451-9. http://dx.doi.org/10.1016/j.ijheatmasstransfer.2008.07.003.
23. Quaresma JMV, Santos CA, Garcia A. Correlation between unsteady-state solidification conditions, dendrite spacings, and mechanical properties of Al-Cu alloys. Metall Mater Trans, A Phys Metall Mater Sci. 2000;31(12):3167-78. http://dx.doi.org/10.1007/s11661-000-0096-0.
24. Kakitani R, Konno C, Garcia A, Cheung N. The effects of solidification cooling and growth rates on microstructure and hardness of supersaturated Al-7%Si-x%Zn alloys. J Mater Eng Perform. 2022;31(3):1956-70. http://dx.doi.org/10.1007/s11665-021-06341-8.
25. Moura DA, Gouveia GL, Gomes LF, Spinelli JE. Understanding the effect of Ni content on microstructures and tensile properties of AlSi10Mg alloy samples under a variety of solidification rates. J Alloys Compd. 2022;924:166496. http://dx.doi.org/10.1016/j.jallcom.2022.166496.
26. Gowri S, Samuel FH. Effect of alloying elements on the solidification characteristics and microstructure of Al- Si- Cu- Mg- Fe 380 alloy. Metall Mater Trans, A Phys Metall Mater Sci. 1994;25(2):437-48. http://dx.doi.org/10.1007/BF02647989.
27. Gerbe S, Krupp U, Michels W. Influence of secondary dendrite arm spacing (SDAS) on the fatigue properties of different conventional automotive aluminum cast alloys. Frat Ed Integrità Strutt. 2019;13:105-15.
28. Fu X, Beatty DN, Gaustad GG, Ceder G, Roth R, Kirchain RE, et al. Perspectives on cobalt supply through 2030 in the face of changing demand. Environ Sci Technol. 2020;54(5):2985-93. http://dx.doi.org/10.1021/acs.est.9b04975. PMid:32072813.
29. Graedel TE, Miatto A. U.S. Cobalt: a cycle of diverse and important uses. Resour Conserv Recycling. 2022;184:106441. http://dx.doi.org/10.1016/j.resconrec.2022.106441.